Title
Antarctic Sea Ice Area in CMIP6

Journal
Geophysical Research Letters, 47(9)

ISSN
0094-8276

Authors
Roach, Lettie A
Dörr, Jakob
Holmes, Caroline R
et al.

Publication Date
2020-05-16

DOI
10.1029/2019gl086729

Peer reviewed

Geophysical Research Letters

RESEARCH LETTER
10.1029/2019GL086729

Antarctic Sea Ice Area in CMIP6

Lettie A. Roach[1], Jakob Dörr[2], Caroline R. Holmes[3], François Massonnet[4], Edward W. Blockley[5], Dirk Notz[2,6], Thomas Rackow[7], Marilyn N. Raphael[8], Siobhan P. O'Farrell[9], David A. Bailey[10], and Cecilia M. Bitz[1]

[1]Atmospheric Sciences, University of Washington, Seattle, WA, USA, [2]Max Planck Institute for Meteorology, Hamburg, Germany, [3]British Antarctic Survey, Cambridge, UK, [4]Georges Lemaître Center for Earth and Climate Research, Earth and Life Institute, Université catholique de Louvain, Louvain-la-Neuve, Belgium, [5]Met Office Hadley Centre, Exeter, UK, [6]Earth System Research and Sustainability (CEN), University of Hamburg, Hamburg, Germany, [7]Alfred Wegener Institute, Helmholtz Centre for Polar and Marine Research, Climate Dynamics, Bremerhaven, Germany, [8]Department of Geography, University of California, Los Angeles, CA, USA, [9]CSIRO Oceans and Atmosphere, Aspendale, Victoria, Australia, [10]Climate and Global Dynamics Laboratory, National Center for Atmospheric Research, Boulder, CO, USA

Key Points:
- CMIP6-mean Antarctic sea ice area is close to observations, but intermodel spread remains substantial
- We find modest improvements in the simulation of sea ice area and concentration compared to CMIP5
- Most CMIP6 models simulate sea ice losses and stronger-than-observed GMST trends over 1979–2018

Supporting Information:
- Supporting Information S1

Correspondence to:
L. A. Roach,
lroach@uw.edu

Citation:
Roach, L. A., Dörr, J., Holmes, C. R., Massonnet, F., Blockley, E. W., Notz, D., et al. (2020). Antarctic sea ice area in CMIP6. *Geophysical Research Letters*, *47*, e2019GL086729. https://doi.org/10.1029/2019GL086729

Received 18 DEC 2019
Accepted 13 MAR 2020
Accepted article online 17 APR 2020

Abstract Fully coupled climate models have long shown a wide range of Antarctic sea ice states and evolution over the satellite era. Here, we present a high-level evaluation of Antarctic sea ice in 40 models from the most recent phase of the Coupled Model Intercomparison Project (CMIP6). Many models capture key characteristics of the mean seasonal cycle of sea ice area (SIA), but some simulate implausible historical mean states compared to satellite observations, leading to large intermodel spread. Summer SIA is consistently biased low across the ensemble. Compared to the previous model generation (CMIP5), the intermodel spread in winter and summer SIA has reduced, and the regional distribution of sea ice concentration has improved. Over 1979–2018, many models simulate strong negative trends in SIA concurrently with stronger-than-observed trends in global mean surface temperature (GMST). By the end of the 21st century, models project clear differences in sea ice between forcing scenarios.

Plain Language Summary Coupled climate models are complex computer programs that simulate the interaction of the atmosphere, ocean, land surface, and cryosphere. An important feature of the Southern Ocean is its sea ice cover, which typically expands in winter to cover an area comparable to that of Russia. Climate models have shown very different amounts of Antarctic sea ice coverage and very different trajectories of sea ice change in response to expected greenhouse gas emissions. This year, new coupled climate models released under the Coupled Model Intercomparison Project (CMIP6) will form the basis of the next IPCC assessment report. Here, we compare output from those models to satellite observations of the areal coverage of sea ice. As a whole, the models successfully capture some elements of the observed seasonal cycle of sea ice but underestimate the summer minimum sea ice area. Compared to results from the previous model generation (CMIP5), the range across models has reduced, and the location of sea ice agrees better with observations. Models project sea ice loss over the 21st century in all scenarios, but confidence in the rate of loss is limited, as most models show stronger global warming trends than observed over the recent historical period.

1. Introduction

Antarctic sea ice area increases sixfold across the austral autumn and winter months in one of the largest seasonal area changes of any surface type on Earth. At the interface between ocean and atmosphere, the sea ice cover determines fluxes of heat, mass, and momentum between these two fluids. Its presence also influences surface albedo, oceanic circulation (Pellichero et al., 2018), and the vulnerability of ice sheets to open ocean forcing (Massom et al., 2018). While Arctic sea ice has clearly decreased over the now 40-year multichannel passive-microwave satellite record, the areal extent of Antarctic sea ice shows a small positive trend over 1979–2018 (Parkinson, 2019). The increase between 2000 and 2014 was several times larger than the increase between 1979 and 1999 (Meehl et al., 2019) but was followed by sudden decreases in recent years, such that the 2017 and 2018 yearly averages were the lowest for the whole 1979–2018 record (Parkinson, 2019). A variety of mechanisms have been proposed for the increase (Armour et al., 2016; Ferreira et al., 2015; Haumann et al., 2014; Holland & Kwok, 2012; Pauling et al., 2017; Purich et al., 2016; Zhang, 2007) and

the decrease (Meehl et al., 2019; Schlosser et al., 2018; Stuecker et al., 2017; Wang et al., 2019), but neither is well understood.

Global coupled climate models can aid our understanding of such climate system variability and provide projections of future climate change. By providing a common model experiment protocol, the Coupled Model Intercomparison Project (CMIP) permits evaluation of climate models developed by 40 or so modeling groups worldwide. As sea ice responds to changes in the atmosphere and ocean, it is often used as a climate diagnostic. Yet despite advances in climate modeling capabilities over recent decades, simulation of Antarctic sea ice has remained a fundamental problem for state-of-the-art climate models (Holmes et al., 2019; Rosenblum & Eisenman, 2017; Roach et al., 2018; Shu et al., 2015; Turner et al., 2013; Zunz et al., 2013). The Intergovernmental Panel on Climate Change (IPCC) Fifth Assessment Report (AR5) concluded that there is "low confidence" in climate model projections for Antarctic sea ice due to "the wide inter-model spread and the inability of almost all of the available models to reproduce the mean annual cycle, interannual variability, and overall increase of the Antarctic sea ice areal coverage observed during the satellite era" (Collins et al., 2013). Similarly, the recent IPCC Special Report on the Oceans and Cryosphere in a Changing Climate found "low confidence" in model ability to explain changes in observed Antarctic sea ice cover (Meredith et al., 2019).

Here we present an initial, high-level evaluation of Antarctic sea ice simulated by models in the sixth phase of the Coupled Model Intercomparison Project (CMIP6, Eyring et al., 2016). We focus on the areal coverage of sea ice, as this quantity can be readily obtained from satellite microwave passive radiometers. We examine the historical mean, interannual variability, and trends in sea ice areal coverage and leave investigation of the processes driving any particular biases to future studies.

2. Methods

The Sea Ice Model Intercomparison Project (SIMIP, Notz et al., 2016) coordinated an evaluation of Arctic sea ice in CMIP6 and established a number of community best practices (SIMIP Community, 2020). In this study, to aid comparison with Arctic results, we adopt similar approaches and diagnostics. Following SIMIP Community (2020), rather than sea ice extent, we principally consider sea ice area (SIA), computed by multiplying sea ice concentration (SIC) with individual grid-cell areas and then summing over the Southern Hemisphere. Here we also include consideration of SIC in the supporting information and for calculation of the integrated ice area error (IIAE). The IIAE, adapted from the extent-based integrated ice-edge error metric (IIEE, Goessling et al., 2016), describes the area of sea ice on which models and observations disagree (Roach et al., 2018). It is the sum of SIA overestimated (O) and underestimated (U),

$$\mathrm{IIAE} = O + U, \tag{1}$$

with

$$O = \int_A \max(c_m - c_o, 0)\delta A \tag{2}$$

and

$$U = \int_A \max(c_o - c_m, 0)\delta A, \tag{3}$$

where A is the area of interest, c_m is the simulated SIC for each model, and c_o is the observed SIC on a common grid. For this computation, we interpolate all data to a regular 1° grid, following Roach et al. (2018).

SIA from satellite observations is calculated from daily SIC data on native grids and then averaged for each month. To sample uncertainty in retrieval algorithms (Ivanova et al., 2014), we use three observational records of SIC: OSI SAF (Lavergne et al., 2019), NASA-Team (Cavalieri et al., 1997), and Bootstrap (Comiso et al., 1997). Differences between the three observational products are greatest at the Southern Hemisphere winter maximum, and the observational spread in the Antarctic is greater than in the Arctic (Figure 1), with the lowest year-round SIA coming from the NASA-Team product. To sample uncertainty in observational products for global mean surface temperatures, we use the mean of four—Berkeley (Rohde et al., 2013), NOAA globaltemp v5.0.0 (Vose et al., 2012), GISTEMPv4 (GISTEMP Team, 2019; Lenssen et al., 2019), and HadCRUT4.6.0.0 (Morice et al., 2012)—following SIMIP Community (2020).

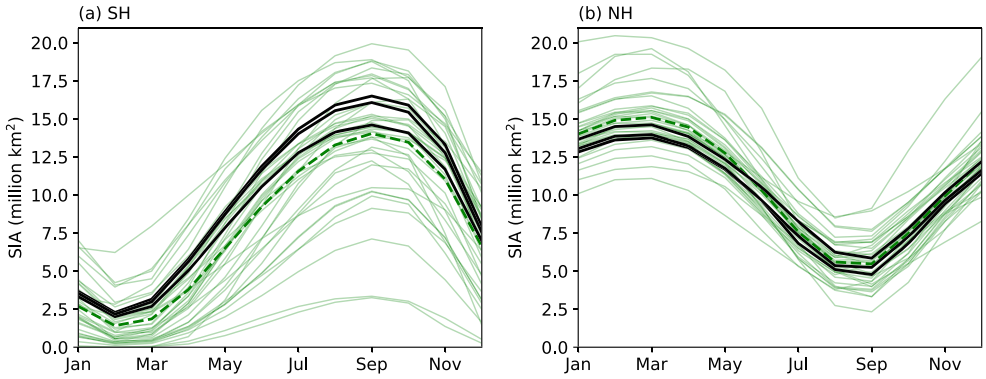

Figure 1. The 1979–2014 mean seasonal cycle in SIA for the CMIP6 r1-ensemble (faint green lines), the CMIP6 multimodel mean (thick green dashed line), and three observational products (black lines) in (a) the Antarctic and (b) the Arctic.

We use the period 1979–2014 in sections 3.1 and 3.2 to take advantage of the higher number of CMIP6 models available from the historical experiments that end in 2014, resulting in 40 CMIP6 models for comparison to 19 CMIP3 models and 38 CMIP5 models (Tables S1 and S2). Due to the recent variability in observed Antarctic sea ice, in subsection 3.3 we consider trends over 1979–2018, extending the historical experiments with the ScenarioMIP experiments (O'Neill et al., 2016) where available. For this we use the SSP2-4.5 experiments, as these have the largest number of participating models, and scenarios are almost identical until 2020 (Riahi et al., 2017), resulting in 28 CMIP6 models for section 3.3.

So as not to give extra weight to models providing multiple ensemble members, and for consistency with both SIMIP Community (2020) and the sea ice analysis in IPCC AR5 (TS.SM.7.2, IPCC, 2013), we generally consider the first ensemble member for each ensemble. We refer to the "CMIPx r1-ensemble" as having one ensemble member from each contributing model and refer to individual ensembles as being the contributions from each CMIP model. All available members from individual ensembles are used only to calculate internal variability in mean SIA in subsection 3.1 and to show internal variability in SIA trends in subsection 3.3. Models are weighted equally although they may share components, a statistical limitation common to CMIP studies. Similarly, individual model ensembles are treated equally here, although methods of ensemble generation vary (cf. Danabasoglu et al., 2020; Golaz et al., 2019). We do not demarcate individual models and observations in the main body of this paper; additional figures showing key metrics for individual models are included in the supporting information.

3. Results

3.1. Mean State (1979–2014)

Figure 1a shows the 1979–2014 mean seasonal cycle in Antarctic SIA from the CMIP6-r1 ensemble. The multimodel mean is lower than the three observational products all year, with the difference from the lowest observational product ranging between 0.4 million km^2 in December and 1.4 million km^2 in May. Two models show a very clear low bias year round, having a lower SIA in winter than many models in summer. There is substantial intermodel spread in Antarctic SIA across the ensemble. Relative to the multimodel mean values, the intermodel standard deviation in Antarctic SIA is more than twice that in the Arctic in corresponding months and is particularly large in austral summer. In spite of the intermodel variance in mean SIA values, all models but one capture the asymmetry in the timing of the Antarctic SIA seasonal cycle, with 5 months retreat and 7 months growth, when considering monthly data in the 1979–2014 mean.

To evaluate CMIP6 simulations in September and February, the typical maximum and minimum months of the seasonal cycle, we consider both the CMIP6 r1-ensemble as a whole (Figures 2a and 2b) and agreement of individual models (Figures S1a and S1b). Estimates of internal variability vary by model, and we cannot judge which is most realistic, so rather than aggregating them in Figures 2a and 2b, we show all estimates individually in Figures S1a and S1b. The three observational products fall within the interquartile range of the CMIP6 r1-ensemble in September, indicating some consistency between the ensemble and observations (Figure 2a). In February, the entire interquartile range is below the observations: a consistent underestimation of summer SIA (Figure 2b). These conclusions hold when accounting for internal variability

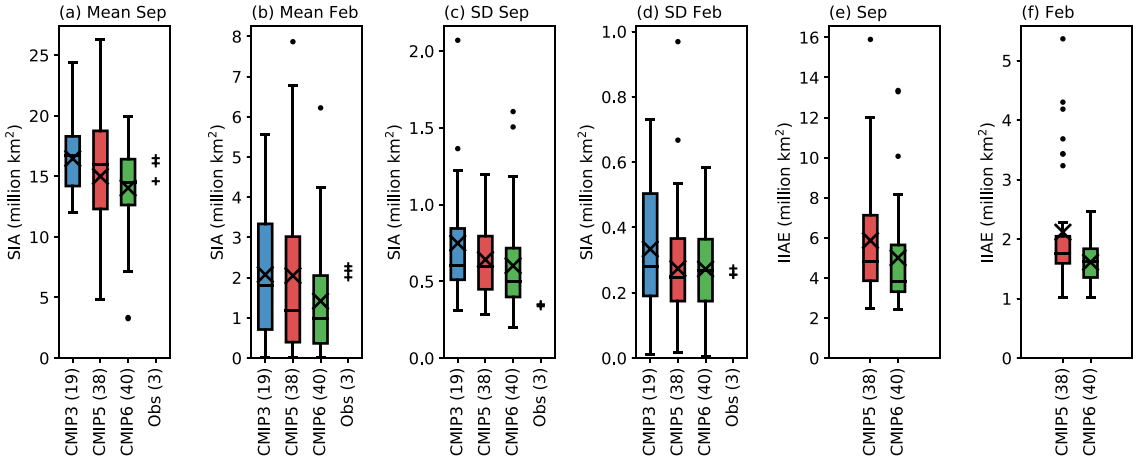

Figure 2. 1979–2014 SIA seasonal cycle statistics for the Antarctic, where boxplots contain one data point per CMIP model in the r1-ensemble. Boxes extend from the lower to upper quartile values of the data with a line at the median and a cross ("X") at the mean. Whiskers show 1.5 times the interquartile range, and data outside this range are considered outliers and shown as circles. The number of models included is noted in brackets. (a) The September mean, (b) the February mean, (c) the September standard deviation of detrended time series, and (d) the February standard deviation of detrended time series (SD), for CMIP3, CMIP5, CMIP6, and the three observational products (marked with +). (e and f) The integrated ice area error (IIAE) from CMIP5 and CMIP6 models in (e) September and (f) February for the 1979–2014 mean, relative to the Bootstrap observations.

(Figures S1a and S1b). As in SIMIP Community (2020), we describe individual models as being consistent with observations if the 1979–2014 mean plus or minus our estimate of internal variability falls within the observed range. Internal variability is estimated as two standard deviations across individual model ensembles with three or more ensemble members and correcting for small sample size, following SIMIP Community (2020), or two standard deviations of the corresponding preindustrial experiment in other cases. Where both calculations are possible, estimates are generally similar (Figures S1a and S1b). Using whichever is the larger estimate, 26 of the 40 CMIP6 models are consistent with observations in September and 16 out of 40 in February (Figures S1a and S1b). Models may achieve consistency with observations by overestimating simulated Antarctic SIA variability, see section 3.2.

Next, we consider Antarctic SIA simulated in CMIP6 relative to two previous generations (Figures 2a and 2b). Comparisons between generations are unlikely to be affected by internal variability, as the probability of choosing an ensemble member that is biased in any particular direction for all models in a generation is low. Besides the 40 CMIP6 models and three observational products, Figures 2a and 2b show the 1979–2014 mean September and February SIA for the 19 CMIP3 models and 38 CMIP5 models. The intermodel spread is large compared to the SIA values, especially in February, and especially for CMIP5, with two CMIP5 models having more than three times the February SIA in observations. Intermodel spread is lower in CMIP6 than CMIP3 and CMIP5 in February and comparable to CMIP3 in September, despite CMIP6 having twice as many models. Multimodel r1-ensemble February mean and median values are below observations for all three model generations but are lowest for CMIP6, indicating that the low bias in summer sea ice has worsened compared to previous CMIP generations.

The regional distribution of Antarctic sea ice is highly variable across CMIP5 (Holland et al., 2017; Roach et al., 2018). Compared to figures from those papers, the spatial distribution of SIC generally appears more uniform across the ensemble, and more similar to observations in CMIP6 (Figures S2 and S3). Several CMIP6 models retain compact summer ice cover (Figure S3), an aspect that was particularly poorly simulated in CMIP5 (Roach et al., 2018). In Figures 2e and 2f, we quantify the spatial distribution of sea ice in September and February using the integrated ice area error (IIAE) over 1979–2014. We show the IIAE relative to the Bootstrap product only; results are similar for the two other observational products. Errors are high relative to the mean SIA values in those months, particularly in February, where in CMIP6 the model-mean IIAE is 1.6 million km^2 and the model-mean SIA is 1.4 million km^2. In both February and September, the multimodel mean and median IIAE are slightly lower in CMIP6 than CMIP5. The model interquartile range in IIAE is similar in CMIP6 and CMIP5, but CMIP6 has fewer outliers with a very high IIAE.

Sea ice thickness is a high-level diagnostic of energy fluxes associated with atmospheric radiation bias, ocean stratification, and heat and mass transport. We show the climatology of sea ice volume per unit grid-cell area (SIVOL), sometimes referred to as "equivalent thickness," across the CMIP6 r1-ensemble in September and February in Figures S4 and S5. The intermodel standard deviation approaches 1 m around the Antarctic Peninsula, where models show the highest SIVOL values. At least a quarter of models show large areas where SIVOL is lower than 0.5m in September (Figure S4) despite having high SIC (Figure S2). Regrettably, the lack of climatological sea ice thickness observations precludes model evaluation.

3.2. Interannual Variability (1979–2014)

Assessments of CMIP5 concluded that models strongly overestimated the interannual variance of Antarctic sea ice extent (Collins et al., 2013; Zunz et al., 2013). Over 1979–2014, observational-mean standard deviations in detrended Antarctic SIA are 0.34 million km^2 in September and 0.26 million km^2 in February. Considering individual (detrended) CMIP6-r1 models over 1979–2014, in February, they are more or less divided equally between having higher and lower interannual variability than observations (Figure S1c). In September, most individual models have higher variability than observations, in some cases exceeding observations by a factor of 4 (Figure S1d).

This aspect is mostly unchanged in CMIP6 from CMIP5 and CMIP3. All three model generations have higher variability than the observations in September and overlap the observations in February (Figures 2c and 2d). Thus, as a whole, models continue to overestimate interannual variability at the winter maximum but appear consistent with observations in terms of variability at the summer minimum over 1979–2014. However, given that the models underestimate summer sea ice area, variability as a fraction of the mean is generally higher in models than observations in February. This result holds over 1979–2018 despite the increase in observed variability over this longer time period (not shown).

3.3. Recent Historical Trends (1979–2018)

The signal of observed change in Antarctic SIA and concentration over 1979–2018 is weak (Handcock & Raphael, 2019; Maksym, 2019; Yuan et al., 2017). SIA trend magnitudes over 1979–2018 are approximately half their 1979–2014 values and vary with observational product by a factor of 2 (Figures 3a and 3b). Assuming a two-tailed t test and using the 95% confidence level as a rough indicator of statistical significance, observed 1979–2018 SIA trends are significant only during winter months (Figure S6). A small dipole pattern of statistically-significant increases and decreases in SIC remains in February, but few significant trends are observed in September (Figures S7 and S8).

Figures 3a and 3b show the observed SIA trends compared to trends in all possible 40-year segments of the CMIP6 preindustrial control runs. A wide range of trends occurs in the absence of greenhouse gas and aerosol forcing. This large variability may be unrealistic, given the overestimation of interannual variability (subsection 3.2). As with CMIP5 (e.g., Polvani & Smith, 2013), observed SIA trends lie well within this range. The more appropriate model-observation comparison, however, is with simulations including anthropogenic forcings similar to those observed, as shown for 1979–2018 (historical simulations extended with SSP2-4.5) in Figures 3c and 3d. In this case, CMIP6 sea ice trends are only marginally consistent with observed SIA trends. The values and significance of SIA trends (Figure S6) and regions of sea ice loss (Figures S7 and S8) vary substantially across the CMIP6 r1-ensemble.

To help explain the modeled trends, Figure 3e shows the linear trend in annual-mean SIA as a function of the annual-mean trend in global mean surface temperature (GMST) over 1979–2018. In contrast to the Arctic (e.g., Gregory et al., 2002; Mahlstein & Knutti, 2012; Winton, 2011), in the Antarctic, the observed correlation between SIA and GMST is weak, while CMIP6 models generally simulate a strong anticorrelation but with substantial across-ensemble variance (Figure 3e). This could suggest that modeled SIA is too dependent on GMST, but equally, it is possible that the observed correlation would be negative and stronger in a world with stronger GMST trends and corresponding sea ice loss. From Figure 3e, models with strong negative trends in SIA also have positive GMST trends much greater than observations—in some cases nearly twice the observed trend. This suggests that at least some of the mismatch with observations may relate to model climate sensitivity, rather than processes specific to the polar regions.

3.4. Twenty-First Century Projections

Finally, we consider SIA time series from 1950 to 2100 (Figure 4), noting that projections should be treated with caution given the model biases discussed above. Figures 4a and 4b show the multimodel means from the

historical and midrange emissions scenarios for the CMIP3, CMIP5, and CMIP6 r1-ensembles (SRESA1B, RCP4.5, and SSP2-4.5, respectively), as this is the scenario with the largest number of model experiments. The rate of change in SIA in February and September is similar across the three generations, but with a slightly higher rate of decline in September in CMIP6 toward the end of the century. CMIP6 has the lowest multimodel mean SIA and, in February, the smallest standard deviation across the multimodel ensemble

Figures 4c and 4d show CMIP6 SIA for the historical experiments and three forcing scenarios: SSP1-2.6, SSP2-4.5, and SSP5-8.5. The scenario multimodel means agree until around 2040 in February and September, reflecting the close agreement of the scenarios in the initial decades (Riahi et al., 2017) and possibly the dominant role of ozone forcing in the first half of the 21st century (Barnes et al., 2014), which is similar across scenarios (Dhomse et al., 2018). Differences between scenario multimodel means are much smaller than intermodel differences within each scenario, reflecting substantial model uncertainty. By the end of the 21st century, there is clear divergence between scenarios in both February and September SIA. In February, the 2090–2099 SSP1-2.6 multimodel mean is 29% lower than the 1979–2014 historical multimodel mean, compared to a loss of over 90% in SSP5-8.5. In September, the losses relative to 1979–2014 are approximately 15% and 50% in scenarios SSP1-2.6 and SSP5-8.5, respectively.

4. Conclusions

In this study, we evaluated sea ice simulated by models from the sixth phase of the Coupled Model Intercomparison Project (CMIP6) using the now 40-year observational record of the areal coverage of sea ice. Sea ice thickness varies across the multimodel ensemble but cannot be evaluated due to the lack of long-term observational references. We have not explored the reasons behind changes in sea ice compared to CMIP5, which may include changes to ocean vertical mixing schemes, multiphase cloud parametrizations, ozone forcing, and increased spatial resolution, including improved bathymetry. Nor have we explored the causes for continued sea ice biases in CMIP6. These may include cloud effects (Kay et al., 2016; Zelinka et al., 2020), spatial resolution that does not permit eddies, which are understood to be highly important for representation of Southern Ocean dynamics (Hallberg & Gnanadesikan, 2006; Poulsen et al., 2018; Rackow et al., 2019), and the lack of coupled ice sheet interactions, which have relevance for the entire Antarctic climate system (Bronselaer et al., 2018; Golledge et al., 2019; Pauling et al., 2017). We anticipate that future studies will investigate these aspects.

Our analysis suggests a smaller discrepancy between models and observations than previously identified due to the extended observational record. Now with four additional years of satellite data, the observed trend in sea ice area has weakened, and the regional signals are less clear over 1979–2018 than 1979–2014. This suggests that natural variability played a major role in the observed trend, as discussed previously (Meehl et al., 2016; Zhang et al., 2019), and that inability of models to reproduce a positive trend should not be used as a criterion to exclude them from projections. Models with the most negative trends in sea ice area are those with large trends in GMST over 1979–2018, in some cases reflecting high climate sensitivity (Zelinka et al., 2020). This suggests that the disagreement with observations in historical sea ice trends is related more to climate forcing than sea ice physics. Using the CMIP6 model ensemble in future emissions scenarios, model uncertainty in sea ice area dominates over scenario uncertainty, but multimodel means clearly diverge for the different scenarios by the end of the 21st century.

Considering sea ice area and concentration, we find some modest improvements in simulated Antarctic sea ice from the 40 models available compared to previous CMIP phases. Compared to CMIP5, the regional distribution of sea ice has slightly improved and the intermodel spread in mean sea ice quantities has decreased. CMIP6 models show consistency with observations at the winter maximum in September and a greater number of models retain high-concentration summer sea ice cover than CMIP5. However, they broadly underestimate the summer minimum sea ice area, more so than CMIP5. Interannual variability of sea ice is still generally larger than that observed over the historical period, and many individual models still simulate implausible mean sea ice area, resulting in a large intermodel spread substantially larger than that in the Arctic. While these issues remain, overall, results suggest that we should have moderately higher confidence in simulation of Antarctic climate in CMIP6 than previous generations.

Acknowledgments
We acknowledge the World Climate Research Programme (WRCP), which, through its Working Group on Coupled Modelling, coordinated and promoted CMIP6. We thank the climate modeling groups for producing and making available their model output, the Earth System Grid Federation (ESGF) for archiving the data and providing access, and the multiple funding agencies who support CMIP6 and ESGF. This work was inspired by the Sea Ice Model Intercomparison Project (supported by the WCRP-CliC Project) and AntClim21 (supported by the Scientific Committee on Antarctic Research, SCAR) workshops in 2019. L. R. would like to acknowledge travel funding from the WMO to attend both of these workshops. L. R. and C. M. B. were supported by the National Science Foundation Grant PLR-1643431 and the National Oceanic and Atmospheric Administration Grant NA18OAR4310274. J. D. was supported by the German Ministry for Education and Research through the project "Meereis bei +1.5°C." C. R. H. was supported by Natural Environment Research Council Grant NE/N01829X/1. F. M. is a F.R.S.-FNRS Research Fellow. E. B. was supported by the Joint UK BEIS/Defra Met Office Hadley Centre Climate Programme (GA01101). D. N. was supported by the Deutsche Forschungsgemeinschaft under EXC 2037 "CLICCS - Climate, Climatic Change, and Society" Project 390683824. The CESM project is supported primarily by the National Science Foundation (NSF). This material is based upon work supported by the National Center for Atmospheric Research (NCAR), which is a major facility sponsored by the NSF under Cooperative Agreement 1852977. We thank Doroteaciro Iovino for providing comments on an early draft of the manuscript. Finally are grateful to two anonymous reviewers for their assistance in improving the manuscript. Data availability: All model output is available online (through https://esgf-node.llnl.gov/projects/esgf-llnl/) (Table S1). All observational products are publicly available at the time of writing: OSI SAF from http://www.osi-saf.org/?q=content/sea-ice-products (Lavergne et al., 2019); NASA-Team and Bootstrap from https://nsidc.org/data/g02202 (Meier et al., 2017); Berkeley from https://berkeleyearth.org/data/ (Rohde et al., 2013); NOAA globaltemp v5.0.0 from https://www.ncdc.noaa.gov/noaa-merged-land-ocean-global-surface-temperature-analysis-noaaglobaltemp-v5 (Vose et al., 2012; Zhang et al., 2020), GISTEMPv4 from https://data.giss.nasa.gov/gistemp/ (GISTEMP Team, 2019; Lenssen et al., 2019); and

References

Armour, K. C., Marshall, J., Scott, J. R., Donohoe, A., & Newsom, E. R. (2016). Southern Ocean warming delayed by circumpolar upwelling and equatorward transport. *Nature Geoscience*, *9*(7), 549–554. https://doi.org/10.1038/ngeo2731

Barnes, E. A., Barnes, N. W., & Polvani, L. M. (2014). Delayed Southern Hemisphere climate change induced by stratospheric ozone recovery, as projected by the CMIP5 models. *Journal of Climate*, *27*(2), 852–867. https://doi.org/10.1175/JCLI-D-13-00246.1

Bronselaer, B., Winton, M., Griffies, S. M., Hurlin, W. J., Rodgers, K. B., Sergienko, O. V., et al. (2018). Change in future climate due to Antarctic meltwater. *Nature*, *564*(7734), 53–58. https://doi.org/10.1038/s41586-018-0712-z

Cavalieri, D. J., Parkinson, C. L., Gloersen, P., & Zwally, H. J. (1997). Arctic and Antarctic sea ice concentrations from multichannel passive-microwave satellite data sets: October 1978–September 1995—User's guide. NASA Goddard Space Flight Center Greenbelt, MD, United States: NASA Technical Memorandum 104647.

Collins, M., Knutti, R., Arblaster, J., Dufresne, J.-L. L., Fichefet, T., Friedlingstein, P., et al. (2013). Long-term climate change: Projections, commitments and irreversibility pages 1029 to 1076. In Intergovernmental Panel on Climate Change (Ed.), *Climate Change 2013 - The Physical Science Basis* (pp. 1029–1136). Cambridge: Cambridge University Press. https://doi.org/10.1017/CBO9781107415324.024

Comiso, J. C., Cavalieri, D. J., Parkinson, C. L., & Gloersen, P. (1997). Passive microwave algorithms for sea ice concentration: A comparison of two techniques. *Remote Sensing of Environment*, *60*(3), 357–384. https://linkinghub.elsevier.com/retrieve/pii/S0034425796002209

Danabasoglu, G., Lamarque, J. F., Bacmeister, J., Bailey, D. A., DuVivier, A. K., Edwards, J., et al. (2020). The Community Earth System Model version 2 (CESM2). *Journal of Advances in Modeling Earth Systems*, *2*, 1–35. https://doi.org/10.1029/2019ms001916

Dhomse, S. S., Kinnison, D., Chipperfield, M. P., Salawitch, R. J., Cionni, I., Hegglin, M. I., et al. (2018). Estimates of ozone return dates from Chemistry-Climate Model Initiative simulations. *Atmospheric Chemistry and Physics*, *18*(11), 8409–8438. https://doi.org/10.5194/acp-18-8409-2018

Eyring, V., Bony, S., Meehl, G. A., Senior, C. A., Stevens, B., Stouffer, R. J., & Taylor, K. E. (2016). Overview of the Coupled Model Intercomparison Project Phase 6 (CMIP6) experimental design and organization. *Geoscientific Model Development*, *9*(5), 1937–1958. https://doi.org/10.5194/gmd-9-1937-2016

Ferreira, D., Marshall, J., Bitz, C. M., Solomon, S., & Plumb, A. (2015). Antarctic Ocean and sea ice response to ozone depletion: A two-time-scale problem. *Journal of Climate*, *28*(3), 1206–1226. https://doi.org/10.1175/JCLI-D-14-00313.1

GISTEMP Team (2019). GISS Surface Temperature Analysis (GISTEMP), Version 4. https://data.giss.nasa.gov/gistemp/

Goessling, H. F., Tietsche, S., Day, J. J., Hawkins, E., & Jung, T. (2016). Predictability of the Arctic sea ice edge. *Geophysical Research Letters*, *43*(4), 1642–1650. https://doi.org/10.1002/2015GL067232

Golaz, J. C., Caldwell, P. M., Van Roekel, L. P., Petersen, M. R., Tang, Q., Wolfe, J. D., et al. (2019). The DOE E3SM Coupled Model Version 1: Overview and evaluation at standard resolution. *Journal of Advances in Modeling Earth Systems*, *11*(7), 2089–2129. https://doi.org/10.1029/2018MS001603

Golledge, N. R., Keller, E. D., Gomez, N., Naughten, K. A., Bernales, J., Trusel, L. D., & Edwards, T. L. (2019). Global environmental consequences of twenty-first-century ice-sheet melt. *Nature*, *566*(7742), 65–72. https://doi.org/10.1038/s41586-019-0889-9

Gregory, J. M., Stott, P. A., Cresswell, D. J., Rayner, N. A., Gordon, C., & Sexton, D. M. H. (2002). Recent and future changes in Arctic sea ice simulated by the HadCM3 AOGCM. *Geophysical Research Letters*, *29*(24), 28–1. https://doi.org/10.1029/2001gl014575

Hallberg, R., & Gnanadesikan, A. (2006). The role of eddies in determining the structure and response of the wind-driven Southern Hemisphere overturning: Results from the Modeling Eddies in the Southern Ocean (MESO) project. *Journal of Physical Oceanography*, *36*(12), 2232–2252. https://doi.org/10.1175/JPO2980.1

Handcock, M. S., & Raphael, M. N. (2019). Modeling the annual cycle of daily Antarctic sea ice extent. *The Cryosphere Discussions*, 1–19. https://doi.org/10.5194/tc-2019-203

Haumann, F. A., Notz, D., & Schmidt, H. (2014). Anthropogenic influence on recent circulation-driven Antarctic sea ice changes. *Geophysical Research Letters*, *41*, 8429–8437. https://doi.org/10.1002/2014GL061659

Holland, P. R., & Kwok, R. (2012). Wind-driven trends in Antarctic sea-ice drift. *Nature Geoscience*, *5*(12), 872–875. https://doi.org/10.1038/ngeo1627

Holland, M. M., Landrum, L., Kostov, Y., & Marshall, J. (2017). Sensitivity of Antarctic sea ice to the Southern Annular Mode in coupled climate models. *Climate Dynamics*, *49*(5-6), 1813–1831. https://doi.org/10.1007/s00382-016-3424-9

Holmes, C. R., Holland, P. R., & Bracegirdle, T. J. (2019). Compensating biases and a noteworthy success in the CMIP5 representation of Antarctic sea ice processes. *Geophysical Research Letters*, *46*, 4299–4307. https://doi.org/10.1029/2018GL081796

IPCC (2013). Climate Change 2013: The Physical Science Basis. In T. F. Stocker et al. (Eds.), *Contribution of Working Group I to the Fifth Assessment Report of the Intergovernmental Panel on Climate Change* (1535 pp.). Cambridge, UK and New York, NY: Cambridge University Press.

Ivanova, N., Johannessen, O. M., Pedersen, L. T., & Tonboe, R. T. (2014). Retrieval of Arctic sea ice parameters by satellite passive microwave sensors: A comparison of eleven sea ice concentration algorithms. *IEEE Transactions on Geoscience and Remote Sensing*, *52*(11), 7233–7246. https://ieeexplore.ieee.org/document/6782670/

Kay, J. E., Wall, C., Yettella, V., Medeiros, B., Hannay, C., Caldwell, P., & Bitz, C. (2016). Global climate impacts of fixing the Southern Ocean shortwave radiation bias in the Community Earth System Model (CESM). *Journal of Climate*, *29*(12), 4617–4636. https://doi.org/10.1175/JCLI-D-15-0358.1

Lavergne, T., Sørensen, A. M., Kern, S., Tonboe, R., Notz, D., Aaboe, S., et al. (2019). Version 2 of the EUMETSAT OSI SAF and ESA CCI sea-ice concentration climate data records. *The Cryosphere*, *13*, 49–78. https://doi.org/10.5194/tc-13-49-2019

Lenssen, N. J. L., Schmidt, G. A., Hansen, J. E., Menne, M. J., Persin, A., Ruedy, R., & Zyss, D. (2019). Improvements in the GISTEMP Uncertainty Model. *Journal of Geophysical Research: Atmospheres*, *124*, 6307–6326. https://doi.org/10.1029/2018JD029522

Mahlstein, I., & Knutti, R. (2012). September Arctic sea ice predicted to disappear near 2°C global warming above present. *Journal of Geophysical Research*, *117*, D06104. https://doi.org/10.1029/2011JD016709

Maksym, T. (2019). Arctic and Antarctic sea ice change: Contrasts, commonalities, and causes. *Annual Review of Marine Science*, *11*(1), 187–213. https://doi.org/10.1146/annurev-marine-010816-060610

Massom, R. A., Scambos, T. A., Bennetts, L. G., Reid, P., Squire, V. A., & Stammerjohn, S. E. (2018). Antarctic ice shelf disintegration triggered by sea ice loss and ocean swell. *Nature*, *558*(7710), 383–389. https://doi.org/10.1038/s41586-018-0212-1

Meehl, G. A., Arblaster, J. M., Bitz, C. M., Chung, C. T. Y., & Teng, H. (2016). Antarctic sea-ice expansion between 2000 and 2014 driven by tropical Pacific decadal climate variability. *Nature Geoscience*, *9*(8), 590–595. https://doi.org/10.1038/ngeo2751

Meehl, G. A., Arblaster, J. M., Chung, C. T. Y., Holland, M. M., DuVivier, A., Thompson, L., et al. (2019). Sustained ocean changes contributed to sudden Antarctic sea ice retreat in late 2016. *Nature Communications*, *10*(1), 14. https://doi.org/10.1038/s41467-018-07865-9

HadCRUT4.6.0.0 from https://www.metoffice.gov.uk/hadobs/hadcrut4/ (Morice et al., 2012). Author contributions: L. R. led the study. L. R. and J. D. processed the data and performed the analysis. All authors contributed to the manuscript. S. O., E. B., and T. R. additionally provided model data before they were available on ESGF.

Meier, W. N., Fetterer, F., Savoie, M., Mallory, S., Duerr, R., & Stroeve, J. (2017). NOAA/NSIDC Climate Data Record of Passive Microwave Sea Ice Concentration, Version 3. [NASA Team and Bootstrap variables], NSIDC: National Snow and Ice Data Center, Boulder, Colorado USA [date accessed: 12/2019]. https://doi.org/10.7265/N59P2ZTG

Meredith, M., Sommerkorn, M., Cassotta, S., Derksen, C., Ekaykin, A., Hollowed, A., et al. (2019). Polar regions. In H.-O.Pörtner et al. (Eds.), *IPCC special report on the ocean and cryosphere in a changing climate* .

Morice, C. P., Kennedy, J. J., Rayner, N. A., & Jones, P. D. (2012). Quantifying uncertainties in global and regional temperature change using an ensemble of observational estimates: The HadCRUT4 data set. *Journal of Geophysical Research*, *117*, D08101. https://doi.org/10.1029/2011JD017187

Notz, D., Jahn, A., Holland, M., Hunke, E., Massonnet, F., Stroeve, J., et al. (2016). The CMIP6 Sea-Ice Model Intercomparison Project (SIMIP): Understanding sea ice through climate-model simulations. *Geoscientific Model Development*, *9*(9), 3427–3446. https://doi.org/10.5194/gmd-9-3427-2016

O'Neill, B. C., Tebaldi, C., Van Vuuren, D. P., Eyring, V., Friedlingstein, P., Hurtt, G., et al. (2016). The Scenario Model Intercomparison Project (ScenarioMIP) for CMIP6. *Geoscientific Model Development*, *9*(9), 3461–3482. https://doi.org/10.5194/gmd-9-3461-2016

Parkinson, C. L. (2019). A 40-y record reveals gradual Antarctic sea ice increases followed by decreases at rates far exceeding the rates seen in the Arctic. *Proceedings of the National Academy of Sciences of the United States of America*, *116*(29), 14,414–14,423. https://doi.org/10.1073/pnas.1906556116

Pauling, A. G., Smith, I. J., Langhorne, P. J., & Bitz, C. M. (2017). Time-dependent freshwater input from ice shelves: Impacts on Antarctic sea ice and the Southern Ocean in an Earth system model. *Geophysical Research Letters*, *44*, 10,454–10,461. https://doi.org/10.1002/2017GL075017

Pellichero, V., Sallée, J.-B., Chapman, C. C., & Downes, S. M. (2018). The Southern Ocean meridional overturning in the sea-ice sector is driven by freshwater fluxes. *Nature Communications*, *9*(1), 1789. https://doi.org/10.1038/s41467-018-04101-2

Polvani, L. M., & Smith, K. L. (2013). Can natural variability explain observed Antarctic sea ice trends? New modeling evidence from CMIP5. *Geophysical Research Letters*, *40*(12), 3195–3199. https://doi.org/10.1002/grl.50578

Poulsen, M. B., Jochum, M., & Nuterman, R. (2018). Parameterized and resolved Southern Ocean eddy compensation. *Ocean Modelling*, *124*, 1–15. https://doi.org/10.1016/j.ocemod.2018.01.008

Purich, A., Cai, W., England, M. H., & Cowan, T. (2016). Evidence for link between modelled trends in Antarctic sea ice and underestimated westerly wind changes. *Nature Communications*, *7*, 10,409. https://doi.org/10.1038/ncomms10409

Rackow, T., Sein, V. D., Semmler, T., Danilov, S., Koldunov, V. N., Sidorenko, D., et al. (2019). Sensitivity of deep ocean biases to horizontal resolution in prototype CMIP6 simulations with AWI-CM1.0. *Geoscientific Model Development*, *12*(7), 2635–2656. https://doi.org/10.5194/gmd-12-2635-201

Riahi, K., van Vuuren, D. P., Kriegler, E., Edmonds, J., O'Neill, B. C., Fujimori, S., et al. (2017). The shared socioeconomic pathways and their energy, land use, and greenhouse gas emissions implications: An overview. *Global Environmental Change*, *42*, 153–168. https://doi.org/10.1016/j.gloenvcha.2016.05.009

Roach, L. A., Dean, S. M., & Renwick, J. A. (2018). Consistent biases in Antarctic sea ice concentration simulated by climate models. *The Cryosphere*, *12*(1), 365–383. https://doi.org/10.5194/tc-12-365-201

Rohde, R., Muller, R., Jacobsen, R., Perlmutter, S., & Mosher, S. (2013). Berkeley Earth temperature averaging process. *Geoinformatics & Geostatistics: An Overview*, *01*(02), 1–7. https://doi.org/10.4172/2327-4581.1000103

Rosenblum, E., & Eisenman, I. (2017). Sea ice trends in climate models only accurate in runs with biased global warming. *Journal of Climate*, *30*(16), 6265–6278. https://journals.ametsoc.org/doi/10.1175/JCLI-D-16-0455.1

SIMIP Community (2020). Arctic Sea Ice in CMIP6. *Geophysical Research Letters*, *47*, e2019GL086749. https://doi.org/10.1029/2019GL086749

Schlosser, E., Haumann, F. A., & Raphael, M. N. (2018). Atmospheric influences on the anomalous 2016 Antarctic sea ice decay. *The Cryosphere*, *12*(3), 1103–1119. https://doi.org/10.5194/tc-12-1103-2018

Shu, Q., Song, Z., & Qiao, F. (2015). Assessment of sea ice simulations in the CMIP5 models. *The Cryosphere*, *9*(1), 399–409. https://doi.org/10.5194/tc-9-399-2015

Stuecker, M. F., Bitz, C. M., & Armour, K. C. (2017). Conditions leading to the unprecedented low Antarctic sea ice extent during the 2016 austral spring season. *Geophysical Research Letters*, *44*, 9008–9019. https://doi.wiley.com/10.1002/2017GL074691

Turner, J., Bracegirdle, T. J., Phillips, T., Marshall, G. J., Hosking, J. S., & Scott Hosking, J. (2013). An initial assessment of Antarctic sea ice extent in the CMIP5 models. *Journal of Climate*, *26*(5), 1473–1484. https//doi.org/10.1175/JCLI-D-12-00068.1

Vose, R. S., Arndt, D., Banzon, V. F., Easterling, D. R., Gleason, B., Huang, B., et al. (2012). NOAA's merged land-ocean surface temperature analysis. *Bulletin of the American Meteorological Society*, *93*(11), 1677–1685. https://doi.org/10.1175/BAMS-D-11-00241.1

Wang, Z., Turner, J., Wu, Y., & Liu, C. (2019). Rapid decline of total Antarctic sea ice extent during 2014–16 controlled by wind-driven sea ice drift. *Journal of Climate*, *32*(17), 5381–5395. https//journals.ametsoc.org/doi/10.1175/JCLI-D-18-0635.1

Winton, M. (2011). Do climate models underestimate the sensitivity of Northern Hemisphere sea ice cover? *Journal of Climate*, *24*(15), 3924–3934. https://doi.org/10.1175/2011JCLI4146.1

Yuan, N., Ding, M., Ludescher, J., & Bunde, A. (2017). Increase of the Antarctic Sea Ice Extent is highly significant only in the Ross Sea. *Scientific Reports*, *7*(1), 41,096. https//doi.org/10.1038/srep41096

Zelinka, M. D., Myers, T. A., McCoy, D. T., Po-Chedley, S., Caldwell, P. M., Ceppi, P., et al. (2020). Causes of higher climate sensitivity in CMIP6 models. *Geophysical Research Letters*, *47*, 1–12. https://doi.org/10.1029/2019GL085782

Zhang, J. (2007). Increasing Antarctic sea ice under warming atmospheric and oceanic conditions. *Journal of Climate*, *20*(11), 2515–2529. https://doi.org/10.1175/612\ignorespacesJCLI4136.1

Zhang, L., Delworth, T. L., Cooke, W., & Yang, X. (2019). Natural variability of Southern Ocean convection as a driver of observed climate trends. *Nature Climate Change*, *9*(1), 59–65. https://doi.org/10.1038/s41558-018-0350-3

Zhang, H.-M., Huang, B., Lawrimore, J., Menne, M., & Smith, T. M. (2020). NOAA Global Surface Temperature Dataset (NOAA-GlobalTemp), Version 4.0, NOAA National Centers for Environmental Information [date accessed: 12/2019]. https://doi.org/10.7289/V5FN144H

Zunz, V., Goosse, H., & Massonnet, F. (2013). How does internal variability influence the ability of CMIP5 models to reproduce the recent trend in Southern Ocean sea ice extent?. *The Cryosphere*, *7*(2), 451–468. https://doi.org/10.5194/tc-7-451-2013

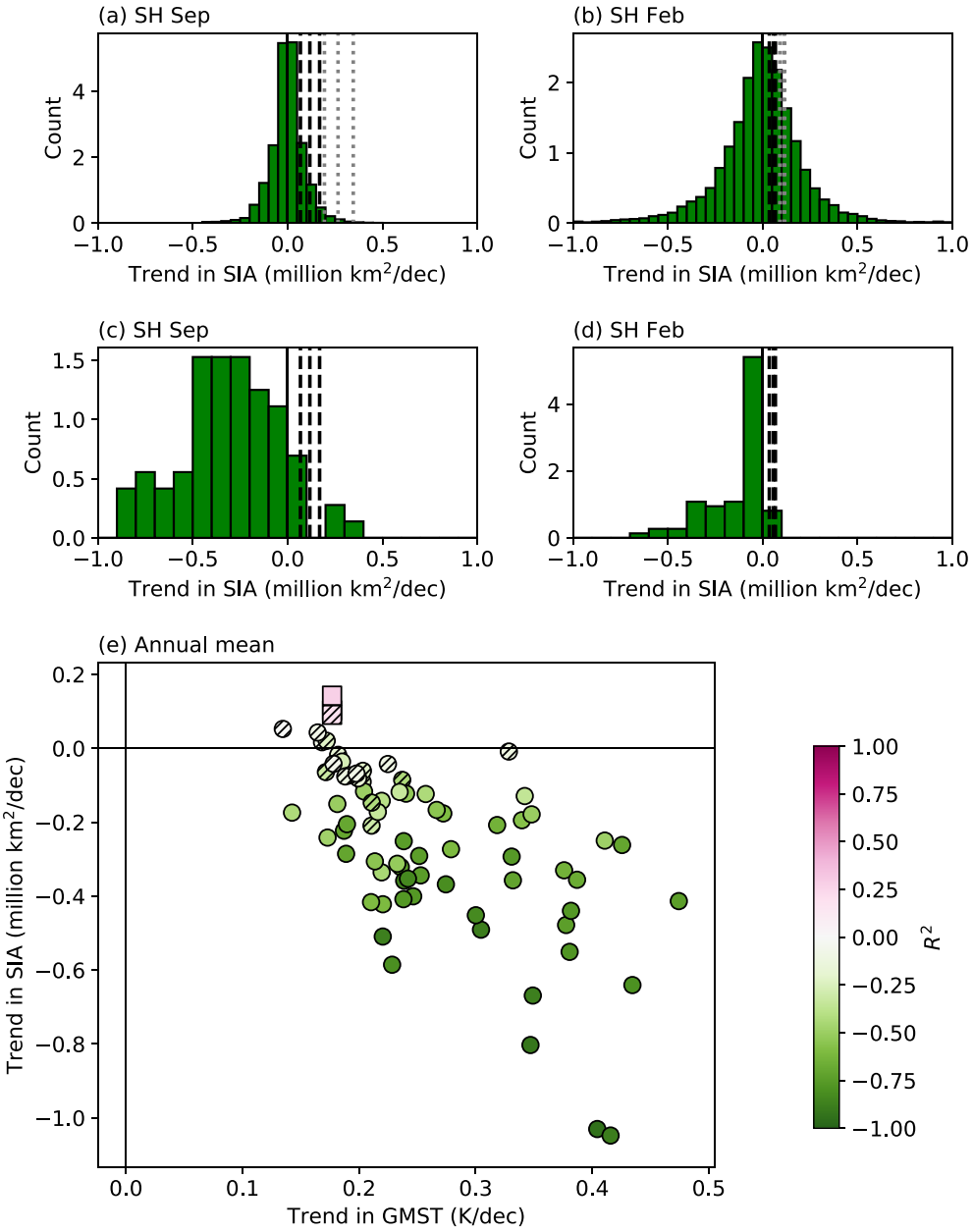

Figure 3. (a and b) Histograms of trends in Antarctic SIA in all possible 40-year segments of CMIP6 preindustrial control runs, calculated from a least squares linear regression and regardless of statistical significance in (a) September and (b) February. Vertical lines show trends in three observational products for (black long-dashed, —) 1979–2018 and (gray short-dashed, -) 1979–2014. (c and d) As (a) and (b) but for CMIP6 historical (forced) experiments extended with SSP2-4.5 over 1979–2018, using all available members from individual ensembles. (e) The linear trend in annual-mean Antarctic SIA over 1979–2018 versus the linear trend in global mean surface temperature over 1979–2018 for (circles) CMIP6 models, including all available ensemble members as individual points, and (squares) observations. The shading indicates the value of the Pearson correlation coefficient between annually varying SIA and GMST. SIA trends that are not statistically significant at the 95% level are hatched. Note that one model (not hatched) lies beneath the observations and is not visible.

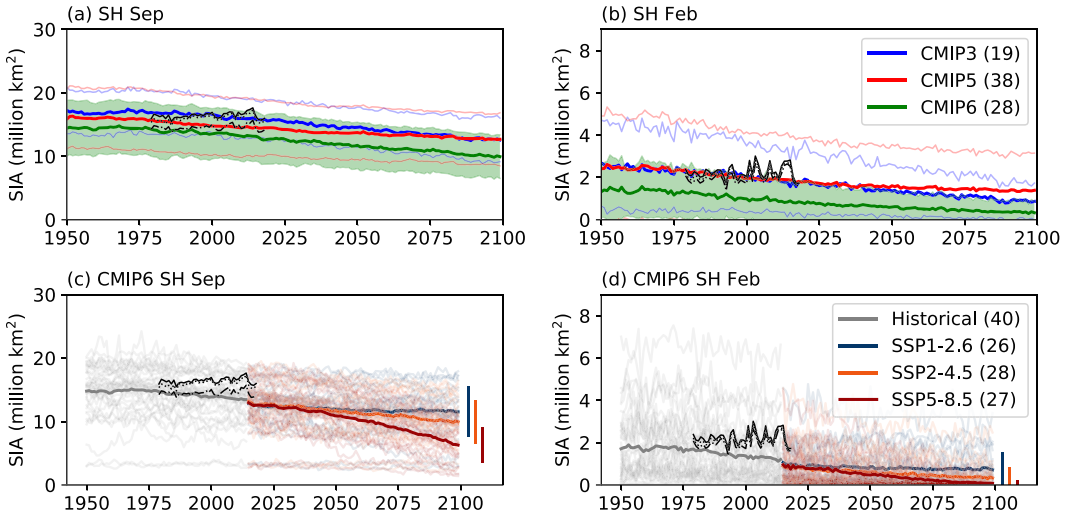

Figure 4. Antarctic SIA time series from 1950 to 2100 in February (b and d) and September (a and c). Upper plots (a and b) show the r1-ensemble means for historical simulations and midrange forcing scenarios: SRESA1B for CMIP3 (blue), RCP4.5 for CMIP5 (red), and SSP2-4.5 for CMIP6 (green). The mean plus or minus one standard deviation across the multimodel ensemble is shown as faint lines or shading corresponding to those colors. Lower plots (c and d) show historical simulations and three scenarios for the CMIP6 r1-ensemble. Thick colored lines denote multimodel means and faint lines show individual model trajectories. The number of models included in each mean is noted in brackets in the legend. In all plots, three observational products are shown in black.